MONITORING THE URBAN HEAT ISLAND PHENOMENON USING THERMAL INFRARED BANDS OF LANDS AT IMAGES FROM 1998 TO 2018, EL-SENBELLAWEEN CITY, EGYPT

Islam H. EL-Gamily[(1)]; Noha S. Donia[(2)] and Hala A. Effat[(3)]
1) National Telecom Regulatory Authority (NTRA) 2) Faculty of Post-Graduate Studies and Environmental Research, Ain Shams University 3)National Authority for Remote Sensing and Space Sciences (NARSS)

ABSTRACT

The continuous development of metropolitan urban areas would lead to an environmental phenomenon known as Urban Heat Island (UHI). It is mainly due to the emission of heat to the lower layer of the atmosphere. UHI was proven to negatively impact human activities in terms of productivity, lifestyle and health issues. It also affects the healthy state of animals and vegetation. The research hypothesis considers that the increase or decrease in the emissivity-corrected Land Surface Temperature (e-corrected LST) in an urbanized area is due to Global Warming (GW), Regional Drivers (RD), and UHI. The study area selected is EL-Senbellaween city located in Dakahliya governorate in the delta of Egypt. It represents the Land Use/Land Cover (LU/LC) changes from cultivated land into an urbanized environment. This research utilized Landsat 5 TM in 1998, 8 Operational Land Imager (OLI) in 2018 and Thermal Infrared Remote Sensor (TIRS) remotely sensed data. Different digital image processing and Remote Sensing (RS) techniques were applied to restore the satellite images and carry out the needed enhancement, analysis, image classification and information extraction. The digital image processing and RS techniques used include calculating the e-corrected LST, LU/LC, Normalized Difference Vegetation Index (NDVI) and UHI. Two GIS-based models were designed and developed using the ArcGIS Pro model

Vol.(50); Iss.(8); No.(5); Aug. 2021
ISSN 1110-0826
Online ISSN 2636-3178

builder tool to calculate the e-corrected LST using TIRS data and then calculate the UHI considering the GW and Regional Drivers effects.

Results indicated that the study area suffers from significant UHI effects. Some changes in LU/LC, such as the changes from vegetation to urban, have a significant negative impact on the climate by more than 13 times the global warming effects.

Keywords: Global Warming (GW), Urban Heat Island (UHI), emissivity-corrected Land Surface Temperature (e-corrected LST)

INTRODUCTION

Remote Sensing (RS) is considered a vital resource in Earth observation. The RS technology utilizes different platforms and sensors mounted on satellites and aircraft to obtain information about objects and features of certain phenomena remotely without direct contact. Remote sensors are passive or active (Tomlinson *et al.*, 2011). RS applications are numerous in different fields including, natural resources management, Agriculture, Geology, Hydrology, study the Land Use/Land Cover, Urban Heat Islands (UHI) and Land Surface Temperature (Sobrino *et al.*, 2004; Navalgund and Roy, 2007; Avdan and Jovanovska, 2016; Simó *et al.*, 2016; El-Hattab *et al.*, 2018).

Thermal Infrared Remote Sensing (TIRS) primarily processes and explains the data acquired in the TIR region of the electromagnetic spectrum. All objects with a temperature above absolute zero emit Thermal Infrared electromagnetic radiation. There is a wide range of applications for the TIR data, such as monitoring Land Surface Temperature (LST). The LST term

Vol.(50); Iss.(8); No.(5); Aug. 2021
ISSN 1110-0826
Online ISSN 2636-3178

usually refers to the radiative temperature that can be felt with the direct touch of different objects on Earth's surface. Avdan and Jovanovska, 2016 created an algorithm for automating LST maps using Landsat 8 OLI satellite data, using Thermal Infrared Band 10. Suresh *et al.*, 2016 succeeded in estimating the LST of the mountain landscape of Devikulma Taluk. They used the Single Window algorithm. They calculated the emissivity based on the Normalized Difference Vegetation Index (NDVI), Band 4 and 5 with 30 m spatial resolution. Sekertekin and Bonafoni, 2020 studied different LST retrieval algorithms using TIR. Their study mainly focused on using Land Surface Emissivity (LSE) as an essential factor that enhances the LST calculation. They applied different methods such as Single Channel Algorithm (SCA), Mono Window Algorithm (MWA), Split Window Algorithm (SWA) and Radiative Transfer Equation (RTE) as effective LST retrieval methods by processing different Landsat imageries (Landsat 5, 7 and 8).

The results indicated that the MWA having a slight accuracy over the rest of the methods used. Hence, the MWA was applied in this study to retrieve the emissivity-corrected LST. Wang *et al.*, 2015 presented an Improved Mono Window Algorithm to calculate the LST from Band 10 data of the Landsat 8 TIR. The algorithm proposed in this study required the use of three parameters: ground emissivity; atmospheric transmittance; and effective mean atmospheric temperature. Rongali *et al.*, 2018 and Wang *et al.*, 2015 only

Vol.(50); Iss.(8); No.(5); Aug. 2021
ISSN 1110-0826
Online ISSN 2636-3178

used the Landsat 8 TIRS Band 10 data, neglecting the TIRS Band 11 data. The reason behind neglecting Band 11 data in calculating LST was that the calibration notification published by the United States Geological Survey (USGS) showed that Band 11 data of Landsat 8 TIR sensor has considerable uncertainty. Hence, It was recommended to use TIRS Band 10 only.

MATERIALS AND METHODS

Study Area: EL-Senbellaween city, located in Dakahliya governorate, Egypt, was selected as the study area for this research. The total approximate area of EL-Senbellaween city is 23 Km^2 (calculated from the administrative boundaries of CAPMAS using ArcGIS Pro v2.8), with a total population of 108,395 inhabitants (as mentioned in the attribute data of the CAPMAS base map of 2017). (fig. 1).

Vol.(50); Iss.(8); No.(5); Aug. 2021
ISSN 1110-0826
Online ISSN 2636-3178

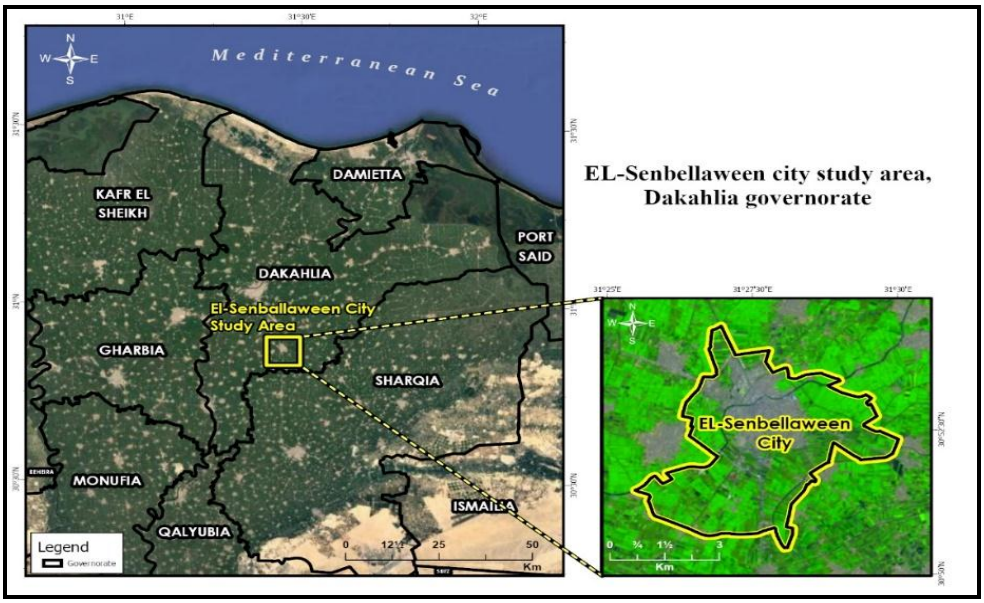

Fig. (1): EL-Senbellaween city study area

The average annual temperature in Dakahlia governorate is 20.5°C, where the average annual rainfall is 56 mm (fig. 2). June has the least amount of rainfall (average of 0 mm), where the most precipitation falls in January with an average of 13 mm. The average temperature measured varies during the year by 13.9°C.

Vol.(50); Iss.(8); No.(5); Aug. 2021
ISSN 1110-0826
Online ISSN 2636-3178

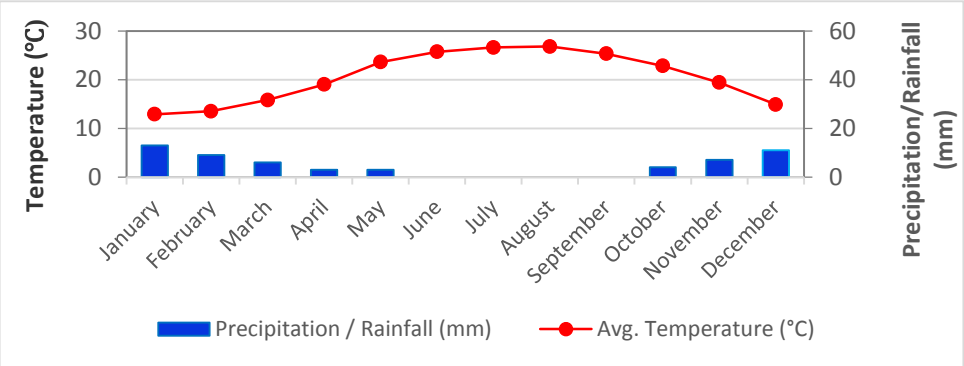

Fig. (2): Climate graph of Dakahliya Governorate (www.Climate-Data.org)

This research integrates RS and Geographic Information System (GIS) technologies to monitor the UHI issue in the study area. The TIR bands of the satellite images will be processed to extract the emissivity-corrected Land Surface Temperature (e-corrected LST) to calculate the UHI effects.

1. SOFTWARE**:** Software packages used in this research study were ERDAS imagine and ArcGIS Pro version 2.8. First, the Landsat imagery Layer Stacking process was applied using ERDAS Imagine. Finally, image classifications and model building were conducted using ArcGIS Pro.

Vol.(50); Iss.(8); No.(5); Aug. 2021
ISSN 1110-0826
Online ISSN 2636-3178

2. DATA**:** The data used in this research were satellite imagery of Landsat 5 (TM) and Landsat 8 (OLI) in August 1998 and August 2018. In addition, optical and TIR Sensor data were utilized. These images were acquired and pre-processed properly. The attribute and spatial data were used, including Administrative Boundaries of Egypt (Governorates, Sectors, and Sub-Sectors).
3. METHODS**:** The layer stacking technique was applied to merge single-band imageries into a single multi-band image, excluding the thermal band. The conceptual model of this research study is as follows:

- Image classification is carried out to produce LU/LC maps.
- Monitor the LST of the study area using thermal bands of Landsat.
- Measure the UHI by applying change detection techniques on both dates.

Fig. (3) shows the conceptual framework of the proposed method applied.

Vol.(50); Iss.(8); No.(5); Aug. 2021
ISSN 1110-0826
Online ISSN 2636-3178

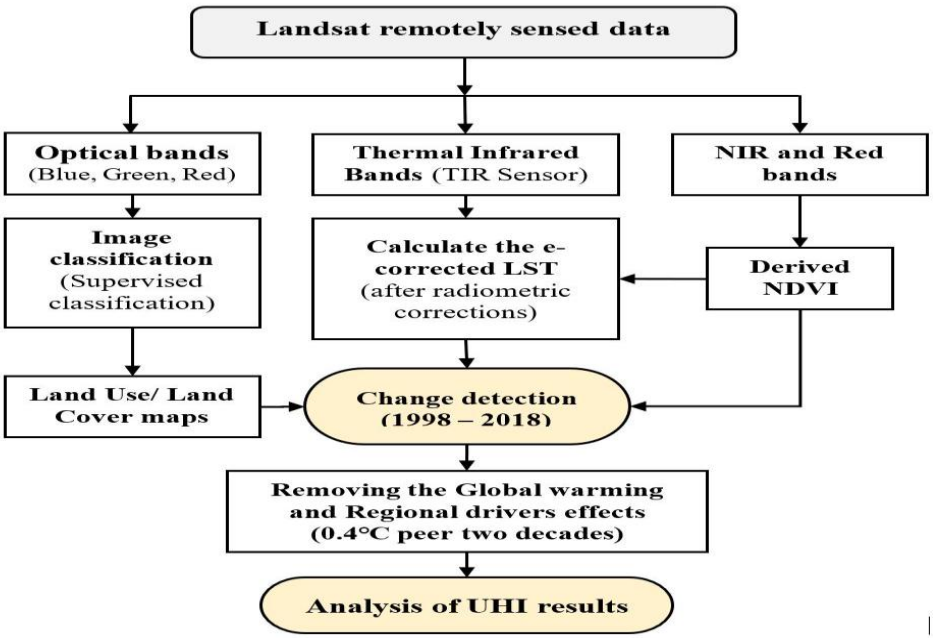

Fig. (3): Process flow diagram of the proposed model to analyze the UHI

In this research study, two main models were designed and developed:

1. Model (1): Calculating the Emissivity-Corrected LST for Landsat 5, Land 7, and Landsat 8 imageries (Fig. 4), and
2. Model (2): Extracting the changes of UHI from 1998 to 2018 (Fig. 5).

Vol.(50); Iss.(8); No.(5); Aug. 2021
ISSN 1110-0826
Online ISSN 2636-3178

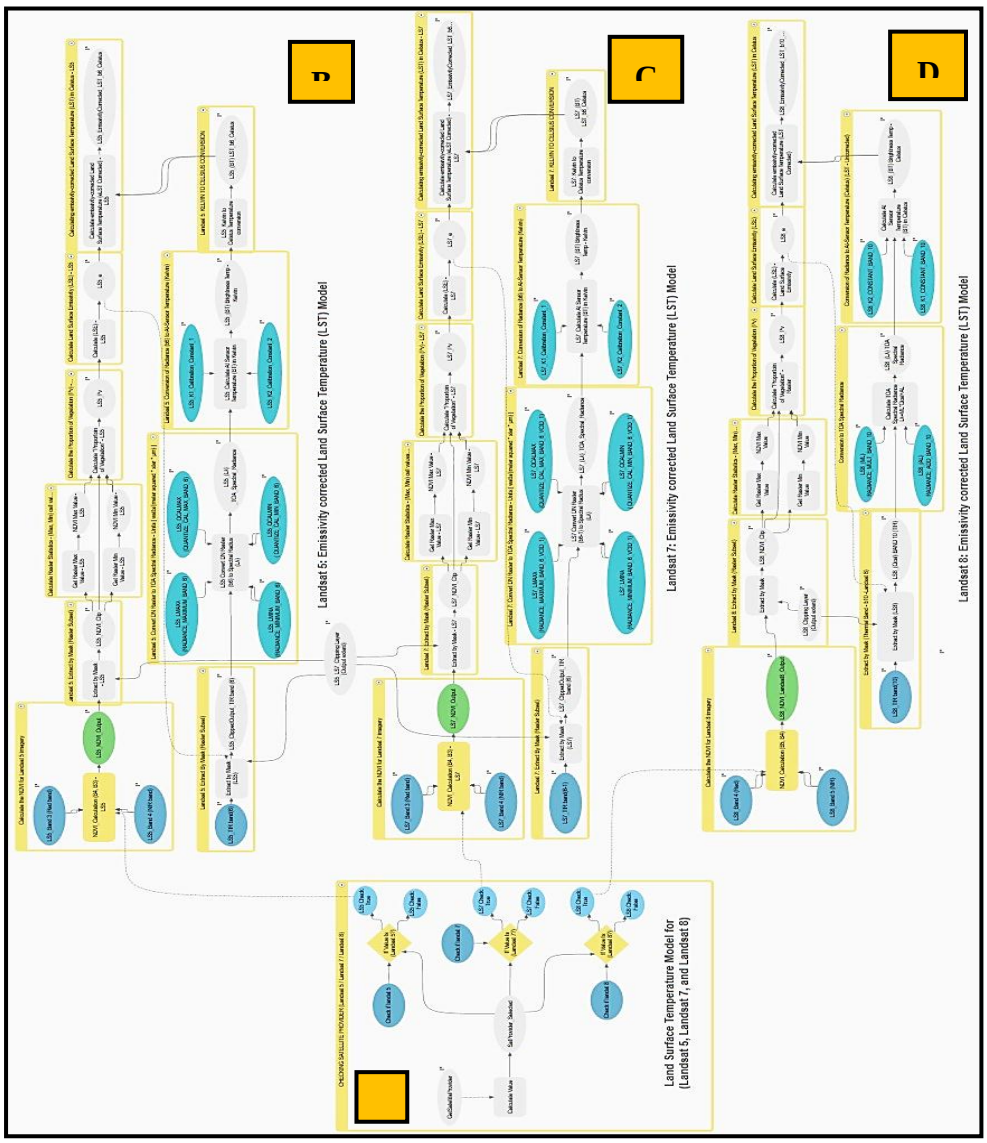

Vol.(50); Iss.(8); No.(5); Aug. 2021
ISSN 1110-0826
Online ISSN 2636-3178

Fig. (4): Emissivity-Corrected LST Complete Model for Landsat 5, 7 and 8 imageries using ArcGIS Pro model builder – Model (1)

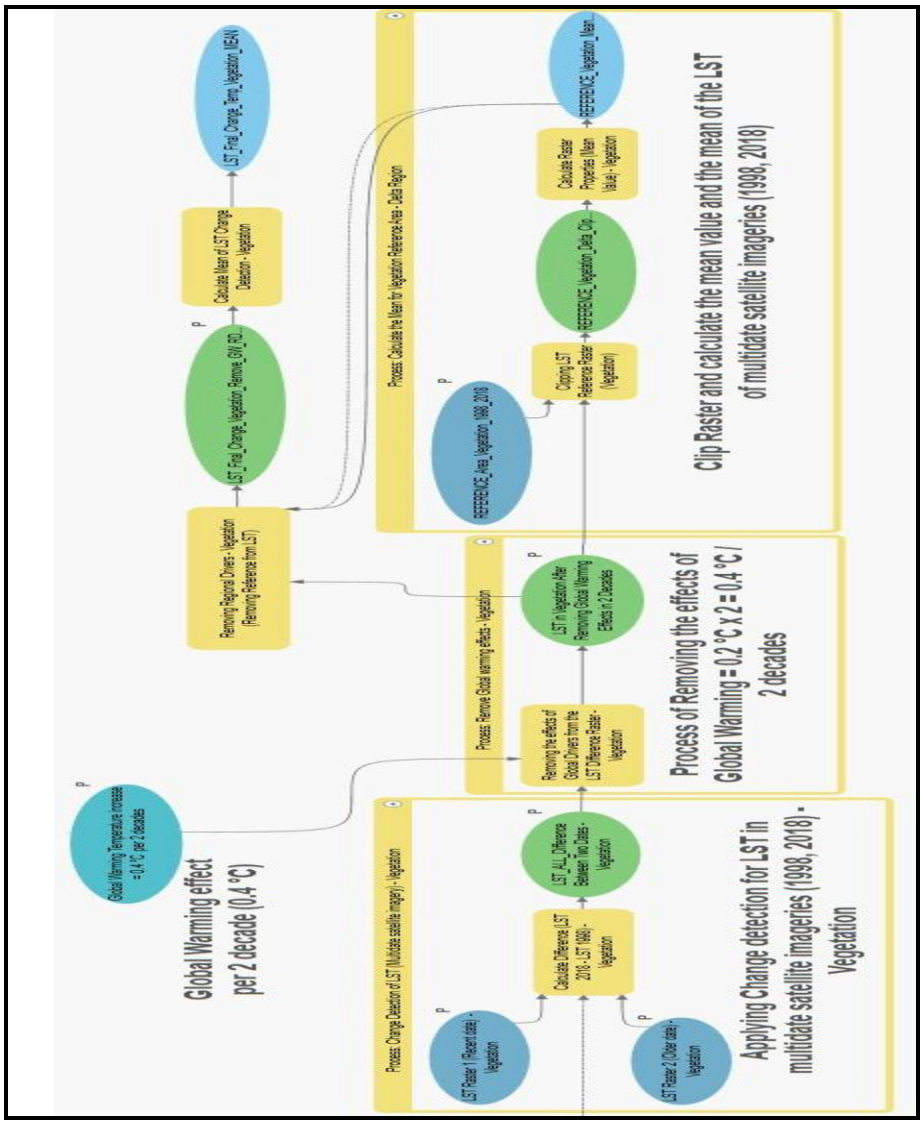

Vol.(50); Iss.(8); No.(5); Aug. 2021
ISSN 1110-0826
Online ISSN 2636-3178

Fig. (5): Change detection Model of UHI after removing the effects of Global Warming and Regional Drivers for both Study Areas using ArcGIS Pro model builder - Model (2)

The process workflow diagram of the Model (1) is referred to as Calculating the Emissivity-Corrected Land Surface Temperature (CECLST) model. This model utilizes the Mono Window Algorithm (MWA) technique to retrieve the e-corrected LST from Landsat TIRS data (Qin and Berliner, 2001; Sobrino *et al.*, 2004; Wang *et al.*, 2015; Rongali *et al.*, 2018; Sekertekin and Bonafoni, 2020). The model output is used as a tool inside the ArcGIS Pro to calculate the e-corrected LST for Landsat images. In addition, Model (1) output is used as input for Model (2), which calculates the UHI by considering Global Warming and regional drivers' effects. Both models were designed and built by the Model Builder module inside ArcGIS Pro (fig. 4 and 5). The equations and techniques applied in Model (1) were introduced by (Qin and Berliner, 2001; Sobrino *et al.*, 2004; Wang *et al.*, 2015; Rongali *et al.*, 2018; Sekertekin and Bonafoni, 2020). The processes of Model (1) are summarized as follows:

- Calculate the Normalized Difference Vegetation Index (NDVI). This indicator is used to measure the health and density of the vegetated areas;

$$NDVI = \frac{R_{NIR} - R_{red}}{R_{NIR} + R_{red}} \qquad \text{(Equation 1)}$$

Where R_{NIR} and R_{red} represent the spectral reflectance of Near-infrared and Red bands, respectively for Landsat 5, 7, and 8 sensors;

Vol.(50); Iss.(8); No.(5); Aug. 2021
ISSN 1110-0826
Online ISSN 2636-3178

- Extract by mask process (for non-thermal bands);
- Retrieve Minimum and Maximum pixel values;
- Calculate the Proportion of Vegetation (P_v) using the following equation

$$P_v = \left(\frac{NDVI - NDVI_{min}}{NDVI_{max} - NDVI_{min}} \right)^2$$ (Equation 2)

Where $NDVI_{min}$ and $NDVI_{max}$ represent the minimum and maximum NDVI;

- Calculate Land Surface Emissivity (LSE) using the following equation

$$LSE = 0.004\ P_v + 0.986$$ (Equation 3)

Where LSE is the Land Surface Emissivity. It was calculated from P_v using the NDVI threshold method proposed by (Sobrino *et al.*, 2004);

- Extract the Thermal bands (band 10 - Landsat 8 & band 6 - Landsat 5);
- Convert Digital Number (DN) to Top-Of-Atmosphere Spectral Radiance.

This process converts DN values to Spectral Radiance and then to Top of Atmosphere reflectance (TOA). The following formula is for Landsat 5:

$$L_\lambda = \left(\frac{\mathrm{LMAX}_\lambda - \mathrm{LMIN}_\lambda}{Q_{cal\ max} - Q_{cal\ min}} \right) * (Q_{cal} - Q_{cal\ min}) + \mathrm{LMIN}_\lambda$$ (Equation 4)

Where;

L_λ = Spectral Radiance at the sensor's aperture [W/(m2 · sr · μm)],

Q_{cal} = Quantized calibrated pixel value which represents thermal band (DN),

Q_{calmin} = Minimum quantized calibrated pixel value (DN = 0) corresponding to $LMIN_\lambda$,

Vol.(50); Iss.(8); No.(5); Aug. 2021
ISSN 1110-0826
Online ISSN 2636-3178

Q_{calmax} = Maximum quantized calibrated pixel value (DN = 255 for sensors TM and ETM) corresponding to $LMAX_\lambda$,

$LMIN_\lambda$ = Spectral at-sensor radiance scaled to $Q_{cal\ min}$ [W/(m2 · sr · μm)],

$LMAX_\lambda$ = Spectral at-sensor radiance scaled to $Q_{cal\ max}$ [W/(m2 · sr · μm)].

For Landsat 8, the TOA spectral radiance (L_λ) is calculated (Equation 5):

$$L_\lambda = M_L \times Q_{cal} + A_L \qquad \text{(Equation 5)}$$

Where:

L_λ = TOA spectral radiance (watts/(m2*ster* μm))

M_L = Band-specific multiplicative rescaling factor obtained from Metadata file (RADIANCE_MULT_BAND_10) = (0.000342)

A_L = Band-specific additive rescaling factor obtained from Metadata file (RADIANCE_ADD_BAND_10) and is equal to (0.1)

Q_{cal} = Quantized and calibrated product pixel values (DN)

- Conversion of Radiance to At-Sensor Temperature (BT) to Celsius using the following formula (equation 5):

$$BT = \frac{K2}{\ln\left(\frac{K1}{L_\lambda}+1\right)} - 273.15 \qquad \text{(Equation 6)}$$

Where;

BT = At satellite brightness temperature in Celsius (°C),

K1 = Thermal Band Calibration Constant 1 in (watts/(meter squared * ster * μm)). K1 is obtained from the metadata files. For Landsat 5, K1 = 607.76 and for Landsat 8 (band 10), K1 = 1321.08.

Vol.(50); Iss.(8); No.(5); Aug. 2021
ISSN 1110-0826
Online ISSN 2636-3178

K2 = Thermal Band Calibration Constant 2. K2 is obtained from the metadata files. For Landsat 5 K2 = 1260.56 Kelvin. Whereas for Landsat 8 (band 10), K2 = 777.89 Kelvin.

L_λ = Top of Atmosphere Spectral Radiance in watts/(m^2 * ster * μm).

- Calculate the e-Corrected LST in Celsius using the following formula:

$$T_s = \frac{BT}{\{1 + [(\lambda * BT/\rho) \ln LSE]\}} \quad \text{(Equation 7)}$$

Where;

T_s = is the emissivity-corrected LST in Celsius (°C);

BT = At satellite Brightness Temperature in Celsius °C;

λ = the wavelength of the emitted radiance of Band 10 (λ = 10.895);

LSE = Land Surface Emissivity calculated in Equation (3); and

$$= h * \frac{c}{\sigma}$$

ρ = 1.438 × 10−2 m K.

Where σ is the Boltzmann constant which is (1.38 × 10−23 J/K), h is the Planck's constant (6.626 × 10−34 J s), and *c* is the speed of light.

Similarly, the main processes included in Model (2) are as follow (fig. 5):

1. Extract the required study area,
2. Apply change detection technique for the e-corrected LST raster data generated from the previous model (Model 1) (for 1998 and 2018),
3. Remove the effects of Global Warming per two decades, which is 0.4°C, from all emissivity-corrected LST data generated from Model (1),

Vol.(50); Iss.(8); No.(5); Aug. 2021
ISSN 1110-0826
Online ISSN 2636-3178

4. Clip the e-corrected LST data and calculate the mean temperature value for the reference area,
5. Remove the Regional Drivers effects from the previous step (changes in the value of the e-corrected LST at the selected reference area. The reference area was identified as a high-density vegetated area in 1998 and still the same in 2018), and
6. Calculate the mean temperature from the LST values.

RESULTS AND DISCUSSION

Satellite Images Processing and Classification: Fig. (6) shows Landsat 5 imagery for the study area in August 1998. The color-composite shown represents the agricultural lands in red. Also, there are some small scattered rural urbanized areas within the agricultural lands. Fig. (7) illustrates the Landsat 8 imagery for the study area in August 2018. In fig. (6), the vegetated lands appear in red. In contrast, fig. (7) shows that more urbanized sites were expanded, and a remarkable increase in scattered rural sites. This expansion indicates that the urbanized areas were exponentially increased in August 2018 at the expense of agricultural lands.

Vol.(50); Iss.(8); No.(5); Aug. 2021
ISSN 1110-0826
Online ISSN 2636-3178

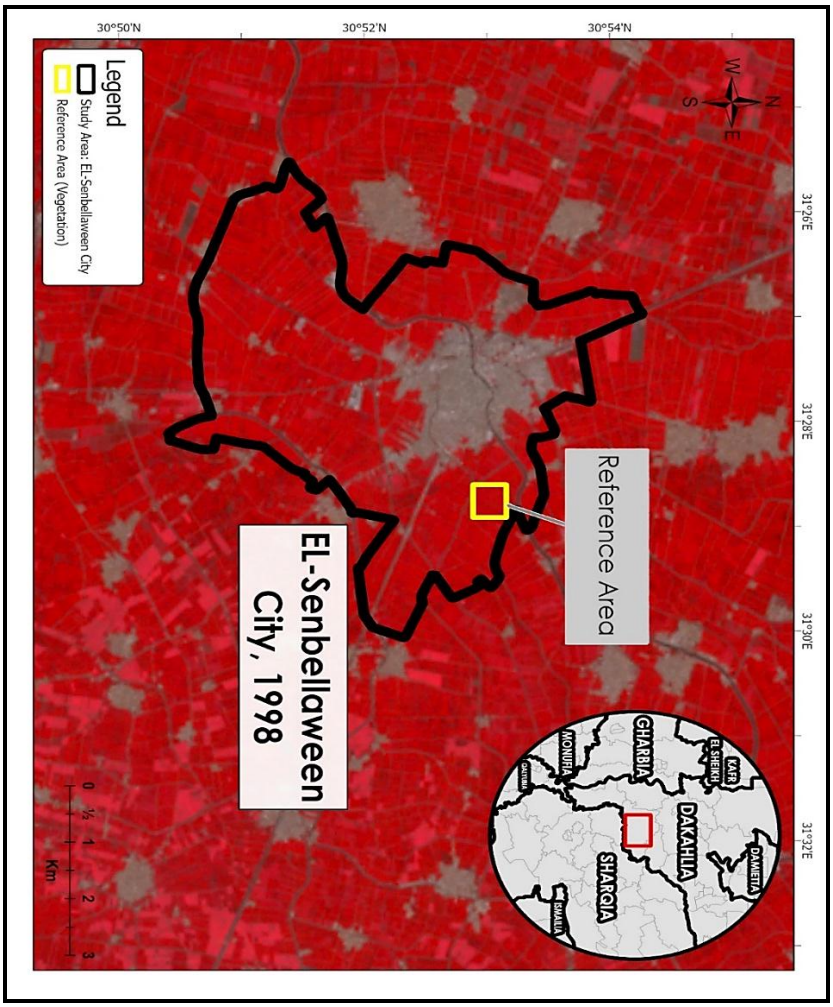

Fig. (6): The false-color composite image of the study area in August 1998 (Landsat-5-TM) (R: band 4 (NIR), G: band 3 (Red), B: band 2 (Green)). The reference area is depicted in the yellow box, and it represents the area with no changes from 1998 to 2018

Vol.(50); Iss.(8); No.(5); Aug. 2021
ISSN 1110-0826
Online ISSN 2636-3178

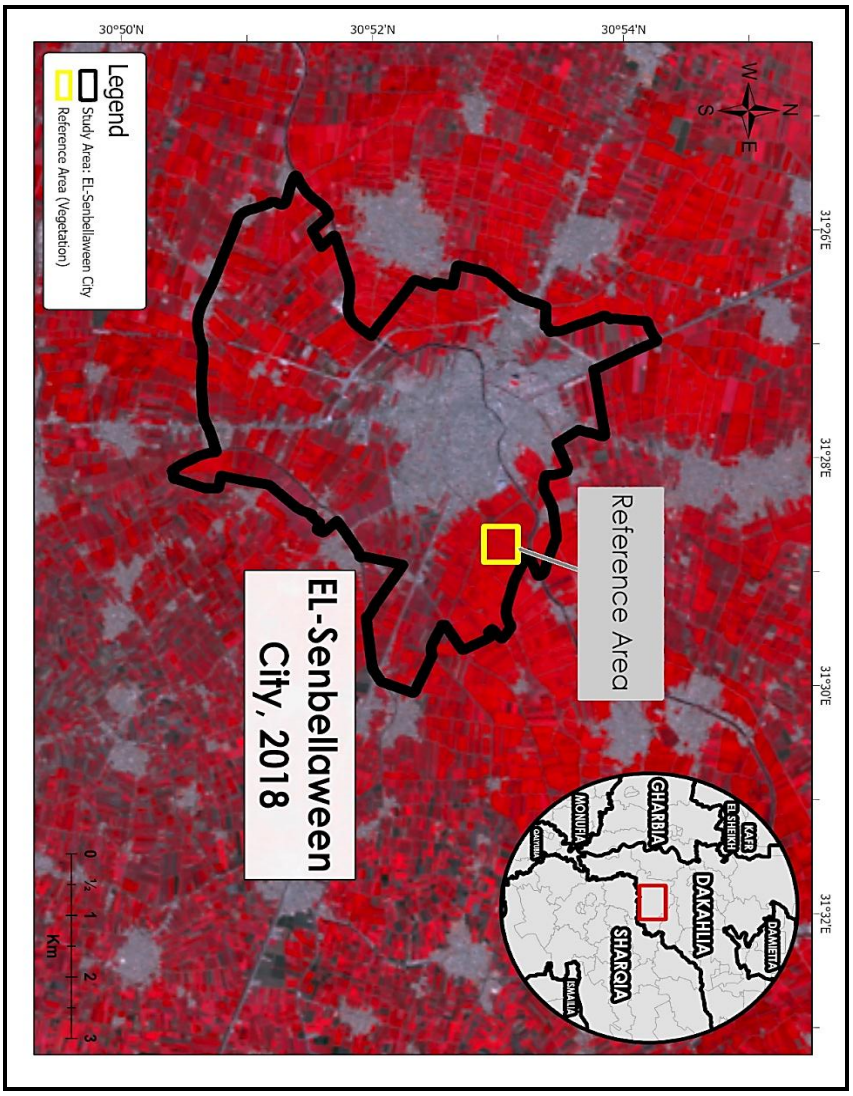

Fig. (7): The false-color composite image of EL-Senbellaween city study area in August 2018 (Landsat-8) (R: band 5 (NIR), G: band 4 (Red), B: band 3 (Green)). The reference area is depicted in the yellow box,

Vol.(50); Iss.(8); No.(5); Aug. 2021
ISSN 1110-0826
Online ISSN 2636-3178

and it represents the area with no changes from 1998 to 2018

The reference area was highlighted with a yellow box in the northern-east of the study area in August 1998 and August 2018 (Fig 6 and 7). This reference area was selected due to no possible LU/LC changes over the years on both dates. Fig. (8) shows the main LU/LC classes in the study areas in August 1998. The brown color represents the urbanized area, while the green color illustrates the vegetated area. The barren soil areas are also represented in light brown, while the water bodies are shown in blue.

The different LU/LC classes areas in August 1998 and August 2018 and their percentages from the total area of EL-Senbellaween city study area were presented in Table (1). It was observed that the urbanized area was doubled (from 3.45 Km^2 to 6.58 Km^2). This increase in the urbanized area was at the expense of the vegetated lands.

Table (1): LU/LC comparison at EL-Senbellaween from 1998 to 2018

Class Name	Area in 1998 (Km^2)	Area (%) in 1998 from total	Area in 2018 (Km^2)	Area (%) in 2018 from total
Water	0.004	0.02%	0.05	0.21%
Urban Area	3.45	14.97%	6.58	28.56%
Vegetation	19.58	84.98%	16.39	71.18%
Soil/Desert	0.01	0.04%	0.01	0.04%

Fig. (9) shows the LU/LC classes at EL-Senbellaween study areas in August 2018. The blue color represents the water bodies; the brown color represents the urbanized area; the green color represents vegetated lands, and

Vol.(50); Iss.(8); No.(5); Aug. 2021
ISSN 1110-0826
Online ISSN 2636-3178

the light brown color represents barren soil areas. Fig. (10) shows the urbanization changes in the study area over 30 years from 1988 to 2018.

Vol.(50); Iss.(8); No.(5); Aug. 2021
ISSN 1110-0826
Online ISSN 2636-3178

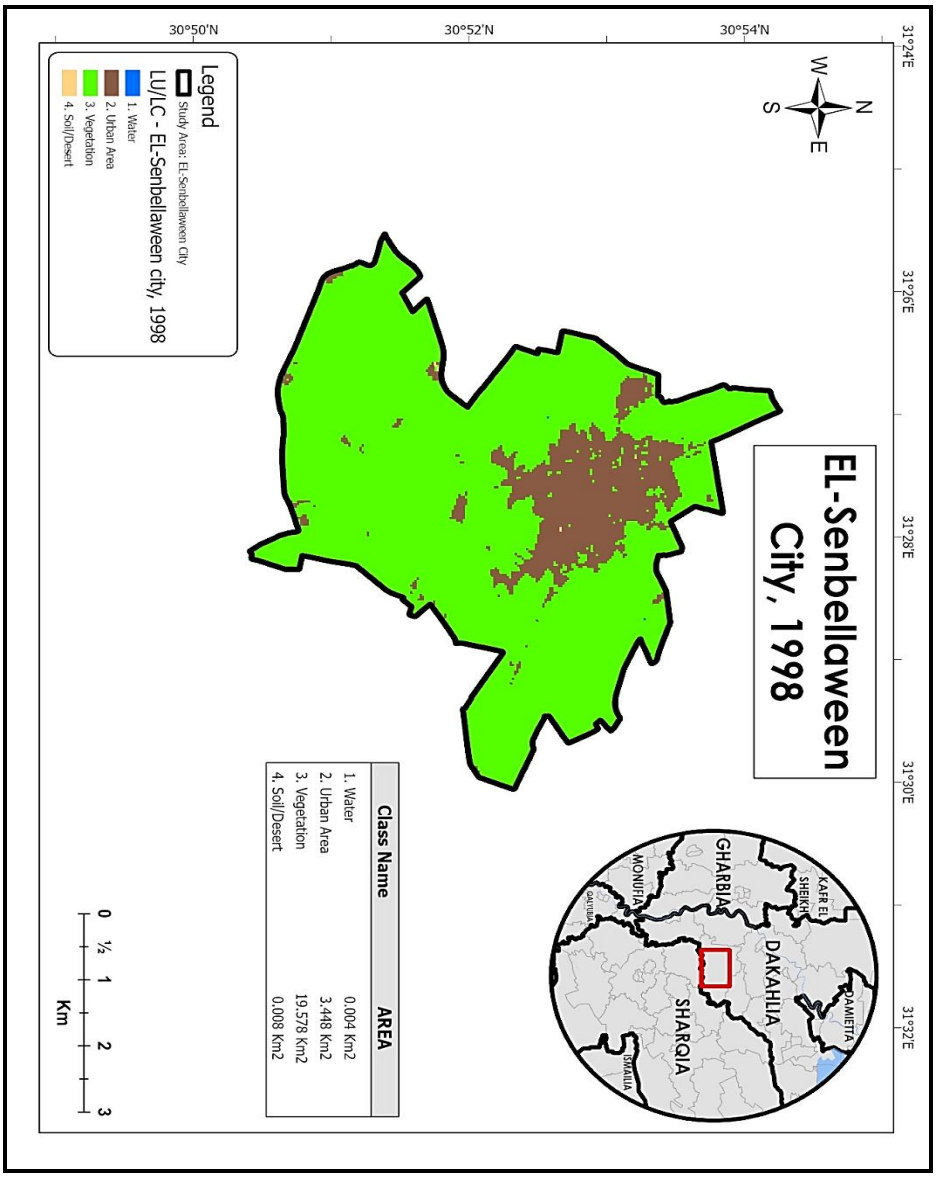

Fig. (8): LU/LC classes of EL-Senbellaween city study area, 1998

Vol.(50); Iss.(8); No.(5); Aug. 2021
ISSN 1110-0826
Online ISSN 2636-3178

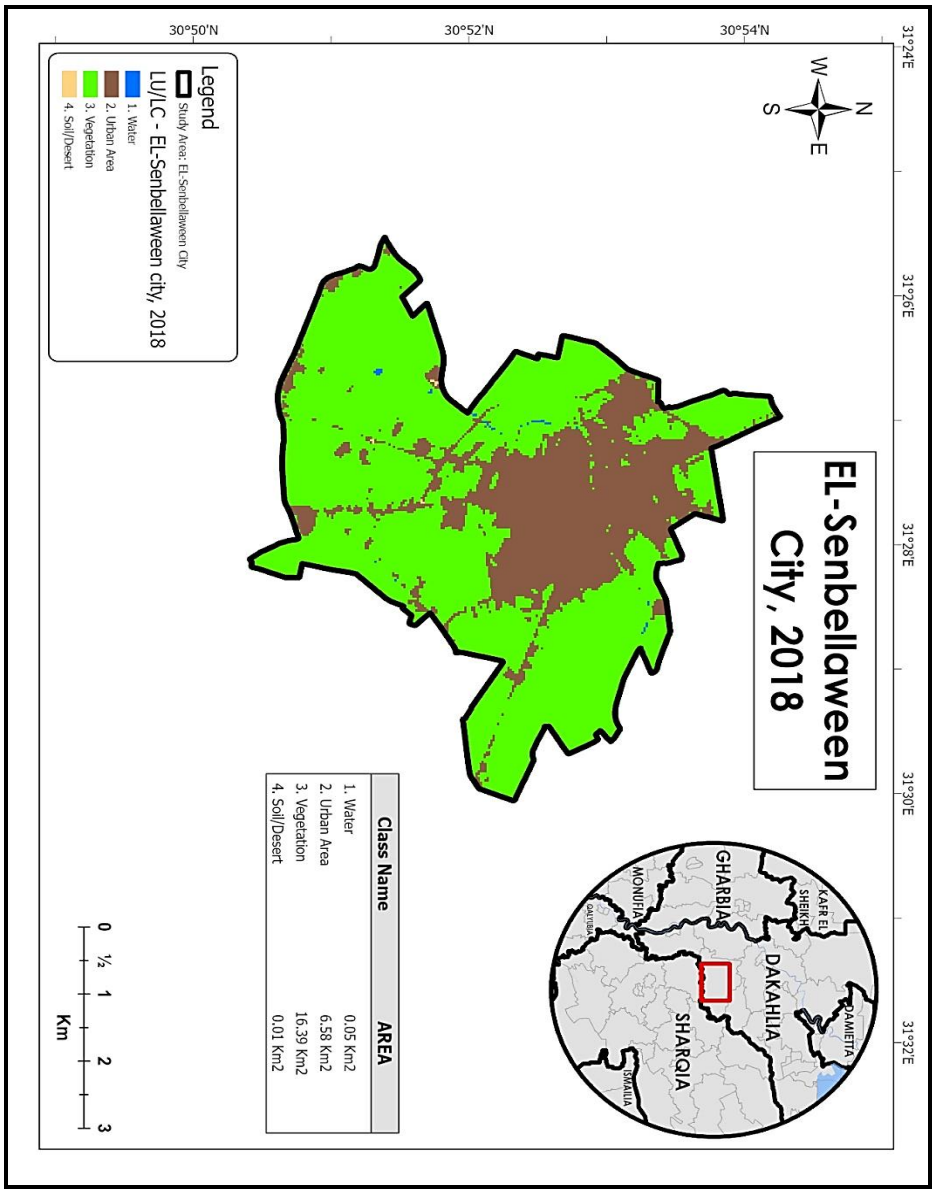

Vol.(50); Iss.(8); No.(5); Aug. 2021
ISSN 1110-0826
Online ISSN 2636-3178

Fig. (9): LU/LC classes of EL-Senbellaween study area, 2018

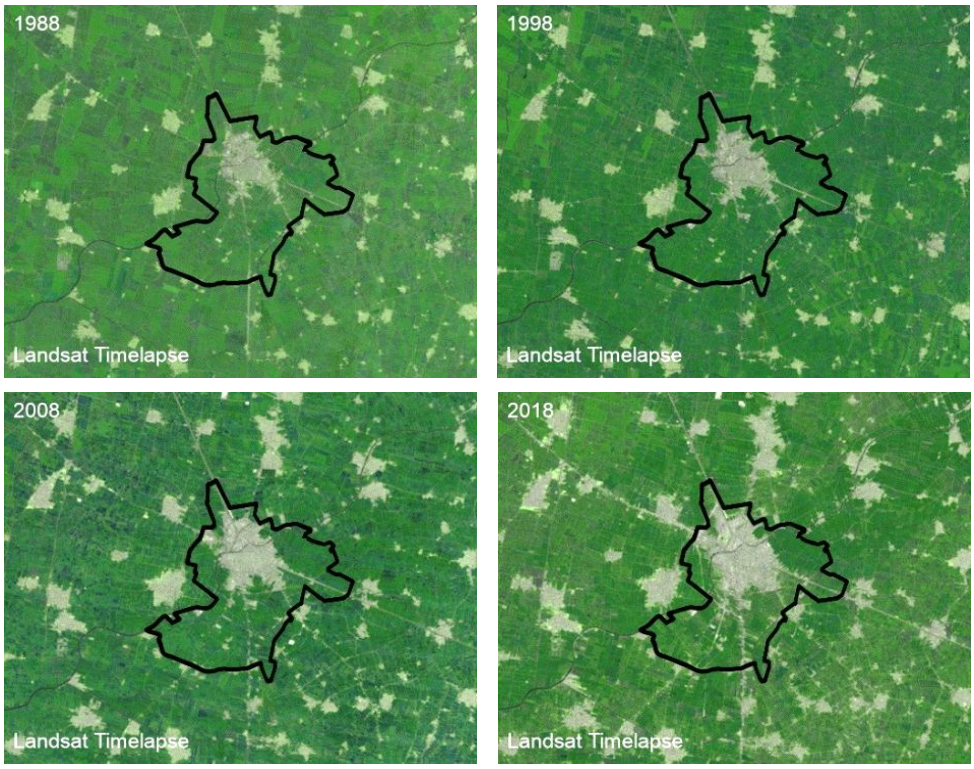

Fig. (10): Change in vegetation and urbanization in EL_Senbellaween study area in 1988, 1998, 2008 and 2018. False-color composite (R: SWIR2, G: SWIR1, B: Red)

THE NDVI RESULT: The NDVI is mainly an indicator that utilizes the Near-Infrared (NIR) bands in the electromagnetic spectrum to assess and analyze healthy vegetated areas. Generally, healthy vegetated areas absorb most of the sun's visible light and reflect a large portion of the NIR to space.

Vol.(50); Iss.(8); No.(5); Aug. 2021
ISSN 1110-0826
Online ISSN 2636-3178

On the other side, barren soils reflect moderately in both the NIR and the red portion of the electromagnetic spectrum (Holm *et al.*, 1987; Sarkar *et al.*, 2011). Therefore, the NDVI values produced are represented as a ratio ranging from -1 to +1. Negative values usually represent water, values around zero represent barren soil, whereas values over 0.6 usually represent green vegetated areas.

Fig. (11) shows the NDVI map for EL-Senbellaween city study area in August 1998 and 2018. Fig. (11 a) illustrates the result of NDVI in the study area and its surroundings in August 1998. It is noticeable that the vegetated areas cover most of the study area and its surroundings. The dark green color represents the dense and healthy vegetated area, while the light green color represents a less dense or less healthy vegetated area. The urbanized areas are presented in brownish gray.

In contrast, fig. (11 b) shows the result of the NDVI in August 2018. The figure shows the expansion of urbanized areas at the expense of the vegetated lands. The high rate of growth of urban and rural slums over the vegetated areas is abnormal. In the study area, the NDVI in August 1998 ranged between -0.006 to + 0.683, whereas in August 2018, the NDVI for the same study area ranged from - 0.037 to + 0.577. This change indicates that cultivated areas were decreased and changed into urbanized and baren soil areas.

Vol.(50); Iss.(8); No.(5); Aug. 2021
ISSN 1110-0826
Online ISSN 2636-3178

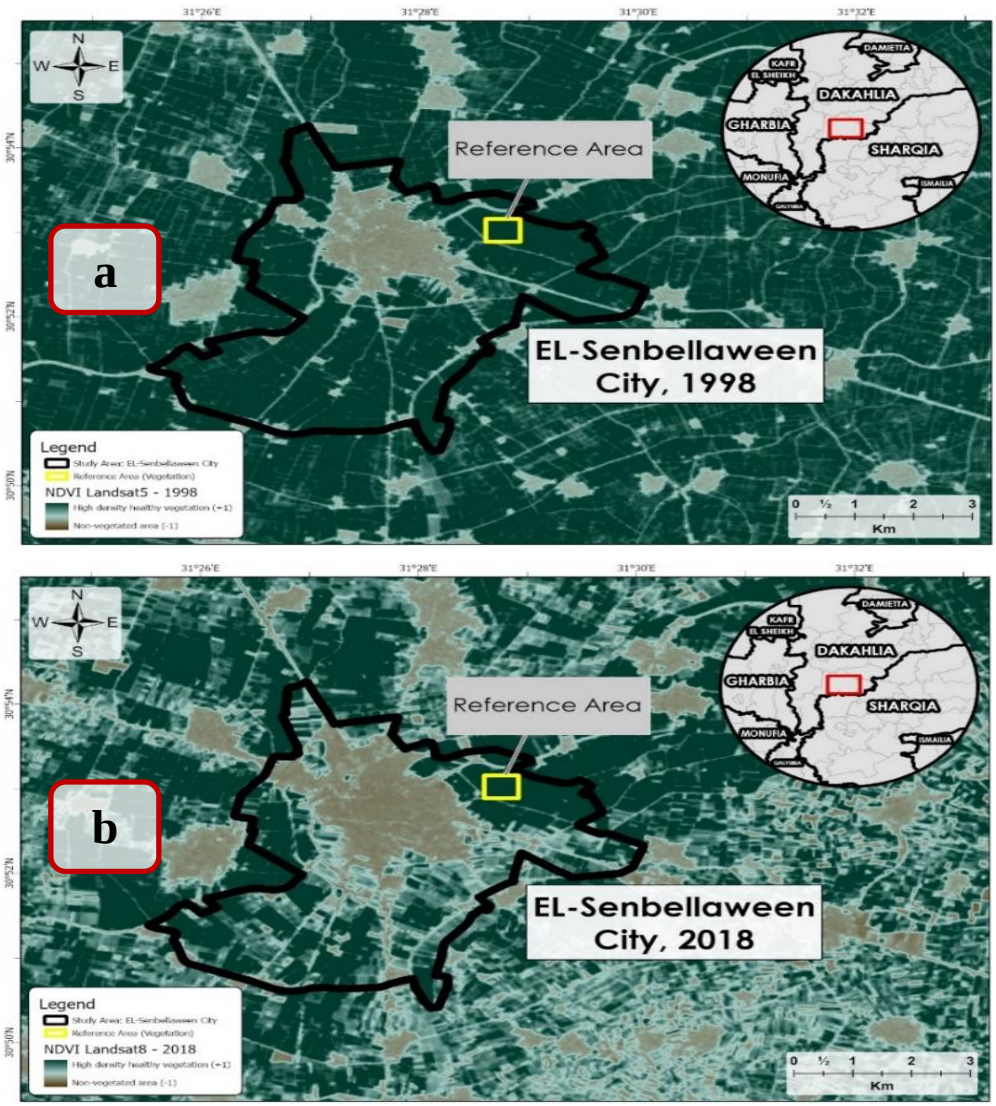

Fig. (11): EL-Senbellaween city study area. The Normalized Difference Vegetation Index (NDVI) in 1998 and 2018. a: NDVI map in

Vol.(50); Iss.(8); No.(5); Aug. 2021
ISSN 1110-0826
Online ISSN 2636-3178

August 1998 b: NDVI map in August 2018

Vol.(50); Iss.(8); No.(5); Aug. 2021
ISSN 1110-0826
Online ISSN 2636-3178

E-CORRECTED LST FINAL RESULTS: Fig. (12) illustrates the calculated e-corrected LST in the study area in August 1998 and 2018. Fig. (12 a) shows the variability of the e-corrected LST in the study area in August 1998. The e-corrected LST of the study area in 1998 ranges from 25.4℃ in the rural and surrounding vegetated areas to 38.4℃ in the urbanized area (Table 2). This variation in the e-corrected LST from rural to urban areas might be due to the low density of urbanization and the high density of vegetation in the rural areas.

Similarly, fig. (12 b) shows the e-corrected LST variability in the study area in August 2018. The e-corrected LST of the study area in 2018 ranges from 27.8℃ in the rural and surrounding agricultural areas to 40.2℃ in the urbanized area (Table 2). The figure shows an increase in the e-corrected LST in both urban and surrounding agricultural areas. This variation might be due to the exponential increase in the density of urbanized areas at the expense of the agricultural areas.

Table (2): The e-Corrected LST in 1998 and 2018 at the study area

Date	e-corrected Minimum LST (°C)	e-corrected Maximum LST (°C)	e-corrected Mean LST (°C)
August 1998	25.4	38.4	28.3
August 2018	27.8	40.2	32.6

Vol.(50); Iss.(8); No.(5); Aug. 2021
ISSN 1110-0826
Online ISSN 2636-3178

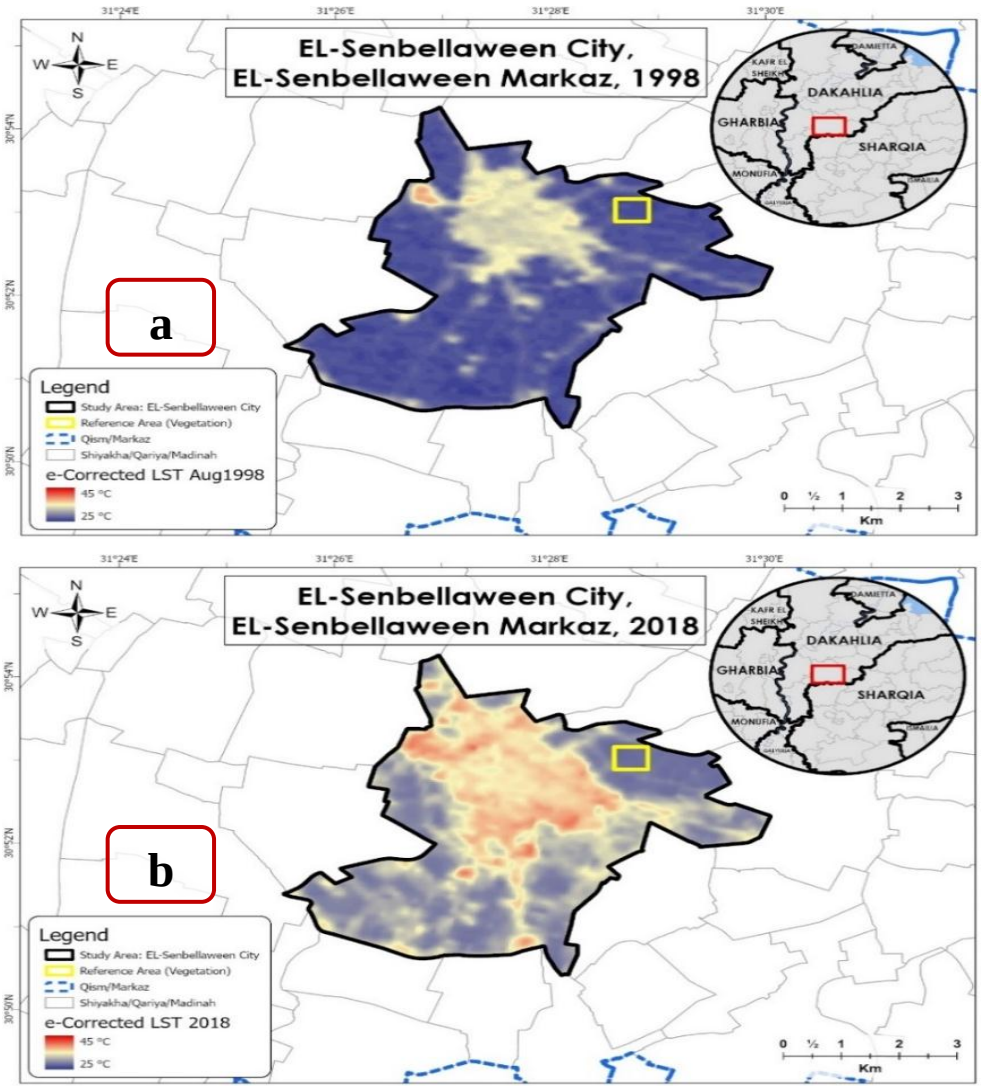

Fig. (12): EL-Senbellaween city study area.
a: The e-Corrected Land Surface Temperature (LST), Aug 1998
b: The e-Corrected LST, Aug 2018

Vol.(50); Iss.(8); No.(5); Aug. 2021
ISSN 1110-0826
Online ISSN 2636-3178

UHI RESULTS AND INTERPRETATION: Fig. (13) illustrates the results of calculating the Urban Heat Islands (UHI) in the study area from August 1998 to August 2018. The yellow, orange and red colors represent UHI in the study area. Where the yellow represents the lowest UHI. In contrast, the dark and light blue colors represent Urban Cool Island (UCI) in the same study area per two decades. The result shows that UHI dominates the majority of the study area. The low, moderate and high dense urbanized areas led to different levels of UHI effects. Low UHI in yellow at the lowest part of the study area is mainly due to the agricultural lands' encroachment. A few UCI spots were observed in the study area; this might be due to the healthy status of the green cover and afforestation in the urbanized areas.

CALCULATE THE UHI AFTER REMOVING THE GLOBAL WARMING AND REGIONAL DRIVERS EFFECTS: Table (3) shows the difference in the e-corrected LST after removing the GW (0.2℃/decade) and RD (0.6℃/decade). The change is ranging from -1.6℃ to +11.6℃ in 20 years. The calculated mean of the UHI in two decades for the whole study area is +2.7℃, which means that the UHI per decade in the study area could be estimated to be +1.35℃. This estimation per decade was based on that the changes in the LU/LC in the study area over the period from 1998 to 2018 considered as a linear change. This hypothesis is based on that the rate of change in urbanization in the study area is within a normal change and no abnormal changes were observed during the period from 1998 to 2018.

Vol.(50); Iss.(8); No.(5); Aug. 2021
ISSN 1110-0826
Online ISSN 2636-3178

The result indicates that UHI dominates the city study area from August 1998 through August 2018. This section aims at studying the LU/LC changes from August 1998 to August 2018 in the study area and calculate the mean values of UHI due to the changes in each LU/LC class. These changes include the change from vegetation to urban, vegetation to water and vegetation to soil.

Table (3): Zonal Statistical Analysis for the UHI in the study area from August 1998 to August 2018 (after removing the Global Warming (GW) and Regional Drivers (RD) effects from the e-corrected LST)

Total Area of the Study area (Km^2)	**MIN change in e-corrected LST (°C) after removing GW and RD**	**MAX change in e-corrected LST (°C) after removing GW and RD**	**MEAN of the UHI per two decade (℃)**	**UHI per decade (℃)**
23	-1.6	+11.6	+2.7	+1.35

UHI: Urban Heat Island LST: Land Surface Temperature

Fig. (14) illustrates the UHI due to the change from vegetation into urban areas from August 1998 through August 2018 in the study area. According to table (4), the changes from vegetation to urban led to a mean change in the e-corrected LST (after removing GW (0.2℃/decade) and RD (0.6℃/decade)) equals to +5.3℃ in two decades. It means that the UHI in the study area equals +2.7℃ per decade. This increase in the e-corrected LST shows that the impact of urbanization on cultivated lands is more than 13 times the global warming effects per decade.

Vol.(50); Iss.(8); No.(5); Aug. 2021
ISSN 1110-0826
Online ISSN 2636-3178

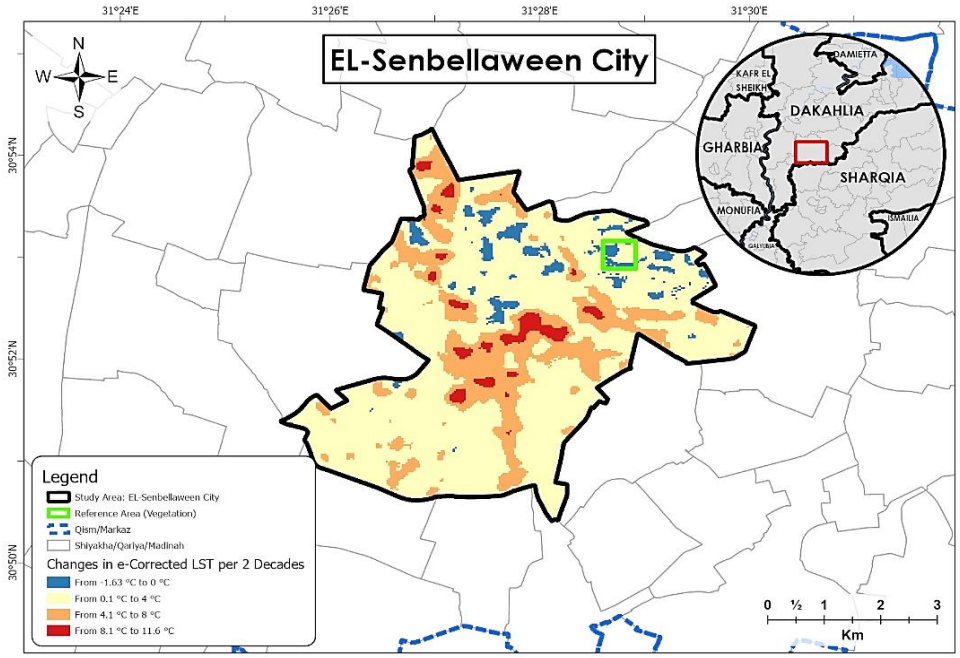

UHI: Urban Heat Island LST: Land Surface Temperature

Fig. (13): Urban Heat Island (UHI) at EL-Senbellaween city study area per two decades (Aug. 1998-Aug. 2018 (after removing the effects of Global Warming and Regional Drivers from the e-corrected LST)

Fig. (15) shows the UHI effects due to the change from vegetation to water and soil areas from August 1998 through August 2018 in the same study area. According to table (4), the changes from vegetation to water led to a mean change in the e-corrected LST (after removing GW (0.2℃/decade) and RD (0.6℃/decade)) equals to +2.2℃ in two decades. Therefore, it means that the UHI in the study area equals +1.1℃ per decade. In contrast, the

Vol.(50); Iss.(8); No.(5); Aug. 2021
ISSN 1110-0826
Online ISSN 2636-3178

changes from vegetation to soil led to a mean change in the e-corrected LST (after removing GW (0.2℃/decade) and RD (0.6℃/decade)) equals to +5.3℃ in two decades. Therefore, it means that the UHI in the study area equals +2.7℃ per decade.

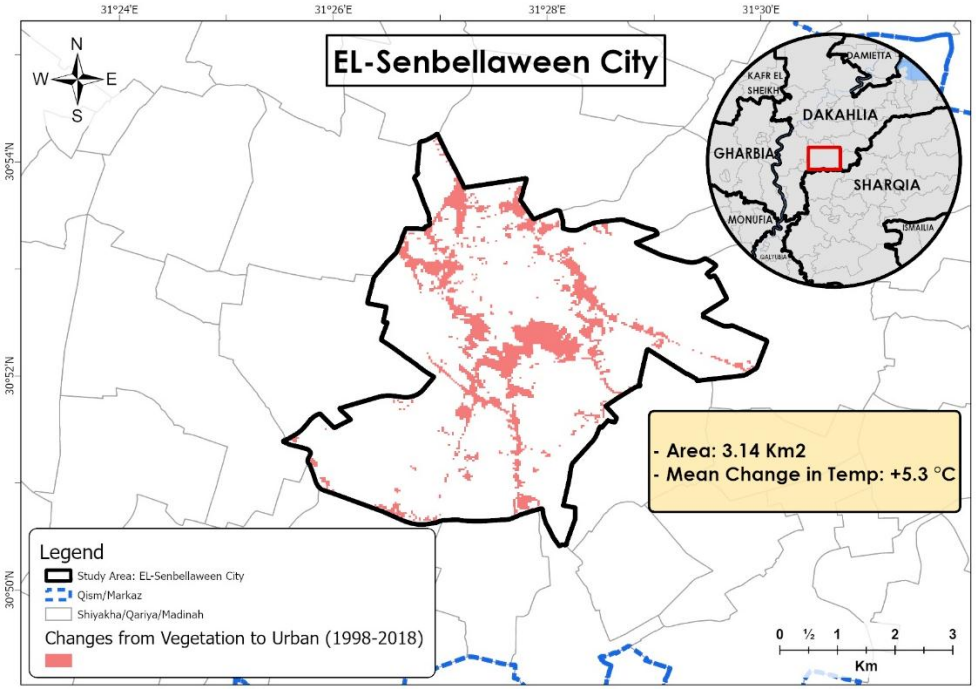

UHI: Urban Heat Island LST: Land Surface Temperature

GW: Global Warming RD: Regional Drivers

Fig. (14): Changes in the e-Corrected LST (℃) from vegetated to urbanized areas in the study area after removing the GW and RD (1998 - 2018)

Vol.(50); Iss.(8); No.(5); Aug. 2021
ISSN 1110-0826
Online ISSN 2636-3178

Table (4): Changes of the e-Corrected LST in the Study area due to change in LU/LC (1998 - 2018) after removing the GW and RD effects

Class Name	AREA (Km2)	MIN change in the e-Corrected LST (°C)	MAX change in the e-Corrected LST (°C)	MEAN change in the e-Corrected LST per two decades (°C)	MEAN Change in the e-Corrected LST per one decade (°C)
Vegetation to Urban	3.14	-1.5	+11.6	+5.3	+2.7
Vegetation to Water	0.04	-0.3	+4.7	+2.2	+1.1
Vegetation to Soil	0.0054	+2.9	+7.7	+5.3	+2.7

LST: Land Surface Temperature

Vol.(50); Iss.(8); No.(5); Aug. 2021
ISSN 1110-0826
Online ISSN 2636-3178

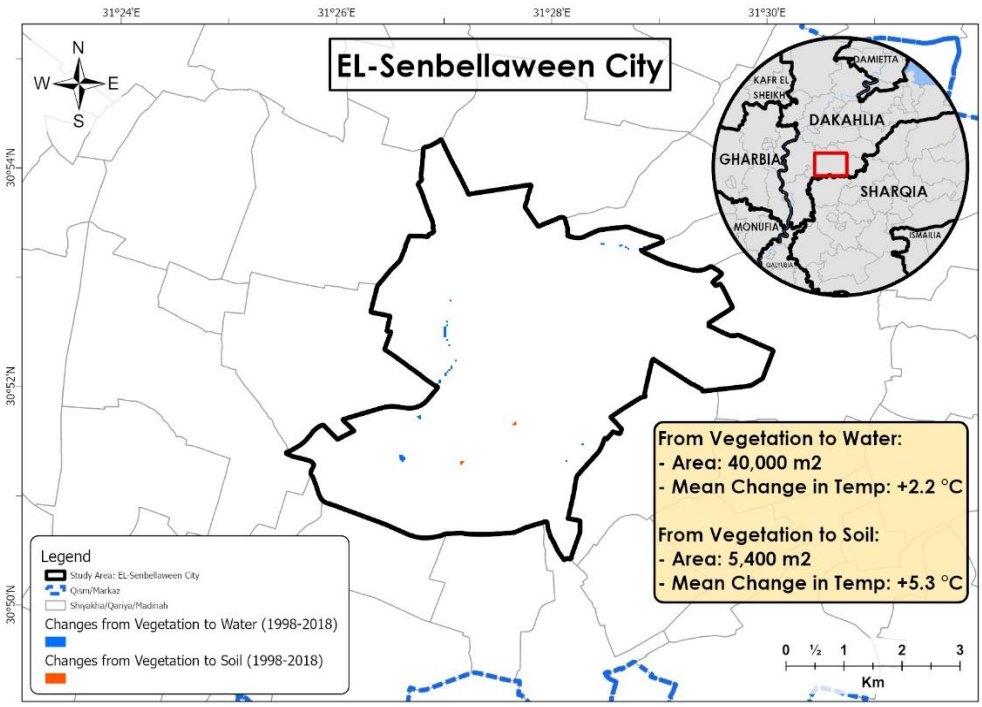

LST: Land Surface Temperature; GW: Global Warming RD: Regional Drivers

Fig. (15): Changes in the e-Corrected LST (℃) from Vegetated to Soil and Water areas in the study area after removing the GW and RD (1998 - 2018)

CONCLUSIONS AND RECOMMENDATIONS

EL-Senbellaween city study area represents most of the cities in the Nile delta and wadis in the style of urbanization. From this study, it can be concluded that the study area suffered from a high rate of urbanization. Most

Vol.(50); Iss.(8); No.(5); Aug. 2021
ISSN 1110-0826
Online ISSN 2636-3178

of the newly urbanized areas are located over agricultural lands that demolish the cultivated lands in wadi and delta over time. The UHI issue has consequences on the climatic change issue. The UHI is mainly due to the expansion of urbanized areas as well as increasing the intensity and anthropogenic activities within these areas. This study concluded that EL-Senbellasween city study area suffered from a negative UHI effect. It is mainly due to the change in the Land Use from vegetation into urban areas. Comparing the values of UHI and the global warming effects per decade in the same study area, it was noticed that the UHI effect is more than 13 times the global warming. So, the UHI issue should be considered more seriously.

The following recommendations are raised out based on this study:

1. Disseminating social awareness regarding the UHI issue and its adverse impacts on humans, climate and biotic environment.
2. The United Nations organizations concerned with the environment should pay more attention and priority to UHI issues similar to or more than the global warming issue.
3. More studies need to be carried out to utilize the recent high-resolution Thermal Infrared remotely sensed data to enhance monitoring and measuring the UHI values.
4. Prohibition of encroachment on agricultural lands especially in the Delta and wadi, and encourage the vertical urbanization concept.

Vol.(50); Iss.(8); No.(5); Aug. 2021
ISSN 1110-0826
Online ISSN 2636-3178

REFERENCE

Avdan, U. and Jovanovska, G. (2016): Algorithm for Automated Mapping of Land Surface Temperature Using LANDSAT 8 Satellite Data. edited by Tian, G. Journal of Sensors, Hindawi Publishing Corporation, 2016, 1480307.

El-Hattab, M., Amany, S. M. and Lamia, G. E. (2018): Monitoring and assessment of urban heat islands over the Southern region of Cairo Governorate, Egypt. Egyptian Journal of Remote Sensing and Space Science, 21(3), 311–323.

Holm, A., Burnside, D. and Mitchell, A. (1987): The development of a system for monitoring trend in range condition in the arid shrublands of Western Australia. The Rangeland Journal, 9(1), 14.

Navalgund, R., V, J. and Roy, P. (2007): Remote sensing applications: An overview. Current Science, Vol. 93.

Qin, Z., Karnieli, A. and Berliner, P. (2001): A mono-window algorithm for retrieving land surface temperature from Landsat TM data and its application to the Israel-Egypt border region. International Journal of Remote Sensing, 22(18), 3719–3746.

Rongali, G., Keshari, A. K., Gosain, A. K. and Khosa, R. (2018): A mono-window algorithm for land surface temperature estimation from landsat 8 thermal infrared sensor data: A case study of the beas river basin, India. Pertanika Journal of Science and Technology, 26(2), 829–840.

Sarkar, T., Ryu, C., Kang, J., Kang, Y., Kim, S., Jeon, S., Kim, W., *et al.* (2011): Integrating geographic information system and remote sensing in predicting rice grain protein, 1–4.

Sekertekin, A. and Bonafoni, S. (2020): Land surface temperature retrieval from Landsat 5, 7, and 8 over rural areas: Assessment of different retrieval algorithms and emissivity models and toolbox implementation. Remote Sensing, 12(2), available at:https://doi.org/10.3390/rs12020294.

Simó, G., García-Santos, V., Jiménez, M. A., Martínez-Villagrasa, D., Picos, R., Caselles, V. and Cuxart, J. (2016): Landsat and local land surface temperatures in a heterogeneous terrain compared to MODIS values. Remote Sensing, 8(10), 1–14.

Sobrino, J. A., Jiménez-Muñoz, J. C. and Paolini, L. (2004): Land surface temperature retrieval from LANDSAT TM 5. Remote Sensing of Environment, 90(4), 434–440.

Suresh, S., V., A. S. and Mani, K. (2016): Mountain Landscape of Devikulam Taluk Using Landsat 8 Data. International Journal of Research in Engineering and Technology, 5(1), 92–96.

Tomlinson, C. J., Chapman, L., Thornes, J. E. and Baker, C. (2011): Remote sensing land surface temperature for meteorology and climatology: A review. Meteorological Applications, 18(3), 296–306.

Wang, F., Qin, Z., Song, C., Tu, L., Karnieli, A. and Zhao, S. (2015): An improved mono-window algorithm for land surface temperature retrieval from landsat 8 thermal infrared sensor data. Remote Sensing, MDPI AG, 7(4), 4268–4289.

Journal of Environmental Sciences (JES)
Faculty of Graduate Studies and Environmental Research, Ain Shams University

رصد ظاهرة الجزر الحرارية باستخدام صور القمر الصناعي لاندسات الحرارية من عام ١٩٩٨ وحتى ٢٠١٨، مدينة السنبلاوين، مصر

إسلام حمدي الجميلي[١]– نهى سمير دنيا[٢]– هالة عادل عفت[٣]
١) الجهاز القومي لتنظيم الاتصالات (NTRA) ٢) كلية الدراسات العليا والبحوث البيئية، جامعة عين شمس ٣) الهيئة القومية للاستشعار من البعد وعلوم الفضاء (NARSS)

المستخلص

إن التوسع المستمر للعمران يؤدي إلى ظاهرة بيئية تعرف باسم "ظاهرة الجزر الحرارية". وترجع هذه الظاهرة إلى انبعاث الحرارة إلى الطبقة السفلى من الغلاف الجوي. وتعكس هذه الظاهرة تأثيرات سلبية على الصحة العامة للإنسان والحيوان والنبات. وتعتمد فرضية هذا البحث على أن الزيادة أو النقصان في درجة حرارة سطح الأرض (بعد تصحيحها) في المناطق الحضرية ترجع إلى كل من تأثير الاحترار العالمي والتأثيرات المناخية الإقليمية نتيجة الأنشطة المختلفة في المناطق المحيطة بالإضافة إلى تأثيرات الجزر الحرارية الناتجة عن النمو العمراني. وتم اختيار منطقة مدينة السنبلاوين كمنطقة دراسة وهي تقع في محافظة الدقهلية شمال مصر. وتمثل منطقة الدراسة هذه التغير في استخدامات الأراضي من أراضي زراعية الى مناطق عمرانية. وفي هذا البحث تم استخدام بيانات مستشعر الأشعة تحت الحمراء الحرارية للقمر الصناعي لاندسات ٥ و ٨. تم إجراء المعالجات المطلوبة لتصحيح وتحسين ومعالجة صور الأقمار الصناعية واستخلاص البيانات والمعلومات المطلوبة. وتضمنت التقنيات المستخدمة في ذلك حساب درجة حرارة سطح الأرض المصححة، وخرائط استخدامات الأراضي والغطاء الأرضي، ومؤشر الغطاء النباتي وحساب درجة الحرارة الناتجة عن ظاهرة الجزر الحرارية. وفي هذا الصدد تم تصميم وتطوير نموذجين يعتمدان على نظم المعلومات الجغرافية لحساب واستخلاص المعلومات الخاصة بقيمة درجة الحرارة الناتجة عن الجزر الحرارية.

وأشارت نتائج هذا البحث إلى أن منطقة الدراسة تعاني من تأثيرات سلبية كبيرة نتيجة ظاهرة الجزر الحرارية. وأظهرت النتائج أن بعض التغيرات في استخدامات الأراضي مثل التغير من أراضي زراعية إلى مناطق عمرانية له تأثير سلبي في زيادة درجة الحرارة أكثر من ثلاثة عشرة مرة من تأثيرات الإحتباس الحراري.

الكلمات الدالة: الإحتباس الحراري، ظاهرة الجزر الحرارية، درجة حرارة سطح الأرض المصححة.

Vol.(50); Iss.(8); No.(5); Aug. 2021
ISSN 1110-0826
Online ISSN 2636-3178